Variational approach to study soliton dynamics in a passive fiber loop resonator with coherently driven phase-modulated external field

Maitrayee Saha,[1,*] Samudra Roy,[1] and Shailendra K. Varshney[2]
[1]*Department of Physics, Indian Institute of Technology Kharagpur, Kharagpur-721302, India*
[2]*Department of Electronics and Electrical Communication Engineering, Indian Institute of Technology Kharagpur, Kharagpur-721302, India*

(Received 4 April 2019; revised manuscript received 6 June 2019; published 1 August 2019)

We report a detailed semianalytical treatment to investigate the dynamics of a single cavity soliton (CS) and two copropagating CSs separately in a Kerr mediated passive optical fiber resonator which is driven by a phase-modulated pump. The perturbation is dealt with by introducing Rayleigh's dissipation function in the framework of a variational principle that results in a set of coupled ordinary differential equations describing the evolution of individual soliton parameters. We further derive closed-form expressions for quick estimation of the temporal trajectory, drift velocity, and the phase shift accumulated by the CS due to the externally modulated pump. We also extend the variational approach to solve a two-soliton interaction problem in the absence as well as in the presence of the externally modulated field. In the absence of a phase-modulated field, the two copropagating solitons can attract, repulse, or propagate independently depending on their initial delay. The final state of interaction can be predicted through a second-order differential equation which is derived by the variational method. While in the presence of the phase-modulated field, the two-soliton interaction can result in annihilation, merging, breathing, or a two-soliton state depending on the detuning frequency and the pump power. Variational treatment analytically predicts these states and portrays the related dynamics that agrees with the full numerical simulation carried out by solving the normalized Lugiato-Lefever equation. The results obtained through this variational approach will enrich the understanding of complex pulse dynamics under a phase-modulated driving field in passive dissipative systems.

DOI: 10.1103/PhysRevE.100.022201

I. INTRODUCTION

Temporal cavity solitons (CSs) are the localized pulse that coexists with a homogeneous continuous-wave (cw) background observed in driven nonlinear passive resonators [1–3]. Unlike the conservative system where nonlinearity balances the pulse broadening due to chromatic dispersion [4], solitons in the dissipative system need an extra balance of energy to compensate for the total loss [5]. The total loss in these dissipative systems is either balanced by an external cw pump or by the presence of an active gain medium. CS was first observed in 2010 in a single mode fiber ring resonator [6] and since then it has gained considerable attention toward all optical buffers [7,8]. They have also been observed in Kerr microresonators, which enables on-chip frequency comb generations [9,10]. Soliton propagation within a resonator under a phase-modulated driving field has received much attention [11–15] because with the minimum modulation depth one can obtain a deterministic way of generating CS without undergoing a chaotic phase. Moreover, it helps to achieve greater control over the generated CS. On the other hand, a theoretical tool depending on the variational approach was first introduced by Anderson [16] for nonlinear pulse propagation; since then it has been used extensively in conservative systems [17–19] as well as in dissipative systems including active [20,21] and passive resonators [22–24] to study the pulse dynamics. In the first part of our study, we performed a detailed analysis of the dynamics of a single CS in the framework of variational treatment and obtained several closed-form expressions of the CS characteristics which can be determined according to the phase profile of the cw. To illustrate this perturbation problem, we numerically solved the Lugiato-Lefever equation (LLE) [25–28] and compared the results obtained with the variational approach.

CSs are generally very robust in nature. One of the key features of CSs is that they can be individually addressed without affecting their nearest-neighbor soliton and several of them can even coexist and propagate independently [2,21,29]. An important limitation may occur if they interfere with each other while propagating. It will disrupt the information of a bit pattern after a few round trips within the cavity. Recently, the bound state (BS) of two solitons in a dissipative passive resonator system has been studied [30,31], where the stable and unstable equilibrium separation between CSs has been attributed by calculating the maxima and minima of their interaction potential. In another article [32], the controlled interaction between two CSs is studied where the merging and annihilation of two solitons are observed against suitable driving strength and frequency detuning. Here, we consider an interaction picture of two CSs both in the absence and in the presence of a phase-modulated driving field in the framework of a variational analysis with the addition of Rayleigh's dissipation function (RDF) [33] that takes into account the

*maitrayee@iitkgp.ac.in

perturbations within the system. Though the phenomena of a single CS dynamics in such a system is well understood in the presence of a phase-modulated driving field, the analytical closed-form expressions for different properties have not been investigated earlier. The closed-form analytical expressions for dynamic pulse parameters are useful in realizing the underpinning physics. Also, our findings would extend the importance of a variational method as a powerful theoretical tool which can handle multisolitons dynamics and even identify the individual effects of internal perturbation (soliton interactions) and external perturbations (phase- or amplitude-modulated driving field). Thus, we believe our findings with this semianalytical technique will help to further deal with several real perturbation situations in the passive dissipative resonator systems complementing various experimental and numerical results.

We organize our work as follows: In Sec. II, we model the localized CS by mean-field LLE and briefly introduce the variational technique. In Sec. III, we discuss the results of a single soliton dynamics under a phase-modulated cw driving field. We assume a cosine-modulated phase profile of the input laser which can be created with an electro-optic modulator and the modulation frequency to be identical with the cavity free spectral range (FSR). Numerical simulations for the dynamics of a single CS are performed with a normalized modified LLE incorporating the phase-modulated pump. The variational technique further describes the results analytically and unfolds the underlying physics. In Sec. IV, we consider the two-soliton interaction dynamics due to a constant driving field with the help of this semianalytical technique. In Sec. V, we investigate various complex dynamics incorporating the above-mentioned two perturbations simultaneously with a fixed delay between the two CSs, i.e., two copropagating CSs under a pump phase-modulated driving field. Stable two-soliton, merged, annihilated, and breathing single-soliton states are formed with a suitable choice of detuning frequency and pump power.

II. GENERAL MODEL

A. Mean-field approach

We consider an optical fiber loop resonator that exhibits Kerr nonlinearity with anomalous dispersion. The evolution of the slowly varying intracavity field envelope $\psi(t,\tau)$ is modeled by the following mean-field LLE [3,25]:

$$\tau_R\frac{\partial\psi}{\partial\tau}=-(\alpha+i\nu)\psi+i\gamma L_c|\psi|^2\psi-i\frac{\beta_2 L_c}{2}\frac{\partial^2\psi}{\partial t^2}+\sqrt{\theta}E_{in}. \tag{1}$$

Here, τ is the normalized slow timescale related with the total evolution time within the resonator, t denotes the normalized fast timescale which characterizes the temporal envelope profile of the generated CS in a reference frame moving at the group velocity of the external driving field, and τ_R is the round-trip time within the cavity. These three timescales can be linked to the round-trip index number m as $E(t=mt_R,\tau)=E^{(m)}(0,\tau)$. The terms in the right-hand side of Eq. (1) signify losses (α), nonlinear phase detuning (ν) of the driving field $E_{in}(t,\tau)$ from the nearest cavity resonance,

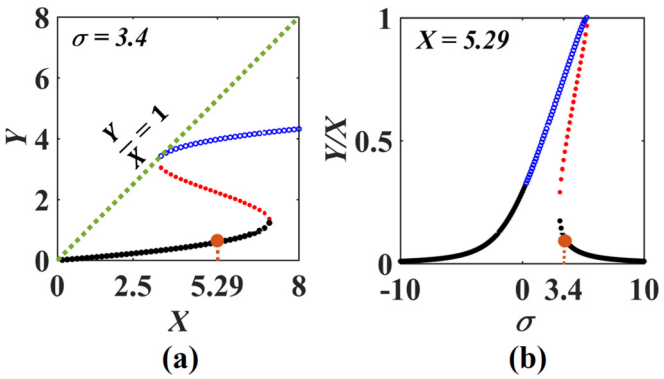

FIG. 1. Optical bistability of the steady and homogeneous state of the intracavity field. (a) Bistability curve showing intracavity power (Y) vs normalized pump power (X); filled circle indicates the chosen pump power for simulation. (b) Ratio of the intracavity power (Y) to pump power (X) vs normalized detuning (σ); tilted under Kerr nonlinearity; filled circle indicates the operating detuning frequency.

γ is the fiber nonlinear coefficient, $\beta_2<0$ signifies second-order anomalous dispersion, E_{in} is the external coherent cw driving field, θ is the power transmission coefficient from the coupler to the resonator, and the length of the resonator is L_c. By introducing the normalization factors $\tau\to\alpha\tau/\tau_R$, $t\to t(2\alpha/|\beta_2|L_c)^{1/2}$, the intracavity field $\psi\to\psi(\gamma L_c/\alpha)^{1/2}$, normalized detuning frequency $\sigma=\nu/\alpha$, and normalized pump $E_{in}\to E_{in}(\gamma L_c\theta/\alpha^3)^{1/2}$, Eq. (1) takes the following form:

$$\frac{\partial\psi}{\partial\tau}=-(1+i\sigma)\psi+i|\psi|^2\psi+i\frac{\partial^2\psi}{\partial t^2}+E_{in}. \tag{2}$$

The steady-state and homogeneous solution of Eq. (2) satisfies the well-known cubic steady-state equation [34] $X=Y^3-2\sigma Y^2+(\sigma^2+1)Y$ with $X=|E_{in}|^2$ and $Y=|\psi|^2$. The steady-state curve is single valued for $\sigma<\sqrt{3}$ and the curve takes an S shape in the case of $\sigma>\sqrt{3}$. It has been calculated in [34] that for $\sigma\geqslant 2$, the power threshold for modulation instability to occur in an anomalous dispersion regime requires $Y>\sigma/2$, which makes the entire upper branch of Fig. 1(a) unstable, so we choose the operating power (filled circle) in the lower stable branch of the bistability curve. Figure 1(b) can be interpreted as the resonance of the ring cavity which is tilted in the presence of the Kerr nonlinearity where we have also marked (filled circle) the operating normalized detuning frequency.

B. Variational approach

We introduce an analytical model which can support the numerical simulation results obtained via the LLE. To analyze a complex situation like soliton interaction in the presence of an external perturbation, we deal with two problems individually with the help of a variational technique. It helps us to gain more insight into the physical parameters of CSs that undergo changes in the presence of a phase -modulated driving field and also due to soliton interactions. The formalism of the variational technique is based on the proper choice of an ansatz function. Though a functional form of a soliton pulse in a dissipative system is presented in [35], we found a rather easy sech ansatz is also suitable to start with

in such dissipative systems which has previously been used in [3,22,23]. Further, we introduce the RDF [33] to handle the perturbations. The construction of the RDF has been performed in such a way that the generalized Euler-Lagrange (EL) equation must reproduce the LLE and its complex conjugate. First, we reduce the problem by inserting the ansatz into Lagrangian and RDF functions. Then, integrating it over fast time t we get $L_g = \int_{-\infty}^{\infty} L\,dt$ and $R_g = \int_{-\infty}^{\infty} R\,dt$. For different perturbation situations the reduced Lagrangian (L_g) remains the same, whereas the reduced RDF (R_g) changes according to the perturbations faced by the CS. Finally, we exploit the EL equation to obtain the equation of motion of different pulse parameters:

$$\frac{d}{d\tau}\left(\frac{\partial L_g}{\partial \dot{p_j}}\right) - \frac{\partial L_g}{\partial p_j} + \left(\frac{\partial R_g}{\partial \dot{p_j}}\right) = 0. \tag{3}$$

Here p_j stands for different pulse parameters (such as amplitude, position, phase, frequency, etc.) and $\dot{p_j} = \frac{dp_j}{d\tau}$.

III. SOLITON PROPAGATION IN A CAVITY WITH PHASE-MODULATED DRIVING FIELD

We consider a situation when the phase of a driving beam is modulated with a cosine profile instead of a constant value and modulation frequency is identical with the resonator free spectral range. Data for numerical simulation is identical to that reported in [32]. The driving field E_{in} of Eq. (2) becomes a function of fast time (t); we assume it is of the form

$$E_{in}(t) = P_{in}\exp\left[iM\chi(t)\right], \tag{4}$$

where $\chi(t) = \cos(\omega t)$, M is the modulation depth, and ω is the modulation frequency. The driving cw field has power P_{in} where its phase is modulated with the help of an electro-optic modulator [11]. For numerical simulations, we use normalized parameters, $\sigma = 3.4$, $P_{in} = 2.3$, $M = 0.15$, $\omega = 0.05$ and we choose our initial wave function of the form $\psi(0,t) = \sqrt{2\sigma}\,\mathrm{sech}[\sqrt{\sigma}(t - t_p)]$; $t_p = 5$. Under phase modulation, the CS undergoes a temporal shift within the resonator.

A. Derivation of the reduced model

To gain more insight, we develop a perturbative theory based on a variational method. We proceed with our analysis using the standard Kerr soliton ansatz [33]:

$$\psi(t,\tau) = \sqrt{2\eta(\tau)}\,\mathrm{sech}\{\sqrt{\eta(\tau)}[t - t_p(\tau)]\} \times \exp(i\{\phi(\tau) - \delta(\tau)[t - t_p(\tau)]\}), \tag{5}$$

where the amplitude ($\sqrt{2\eta}$), phase (ϕ), position (t_p), and frequency shift (δ) are allowed to vary over slow time. Note, the accuracy of the variational method depends on the proper choice of the ansatz. Unlike the Schrödinger Kerr soliton, the CS is formed over a homogeneous pedestal. The given sech ansatz does not include this pedestal and slight misfit from the actual CS as depicted in Fig. 2. Note that in the formalism of the variational method we require an ansatz which is square integrable (i.e., $\int_{-\infty}^{\infty}|\psi|^2 dt < \infty$). It is difficult to form the reduced Lagrangian $L_g(= \int_{-\infty}^{\infty} L dt)$ if the given ansatz contains a constant pedestal. Hence the lack of a pedestal in the sech form may lead to an error in peak power calculation. However, this error can be reduced by eliminating the homogeneous background through the rescaling of field power as $|\psi(t,\tau)|^2 \to |\psi(t,\tau)|^2 - |\psi_h|^2$, where $\psi_h \approx E_{in}\sigma^{-1}(\sigma^{-1} - i)$ is the homogeneous field describing the cw background [3]. Next we construct the Lagrangian (L) and RDF (R) for LLE given in Eq. (2) as follows:

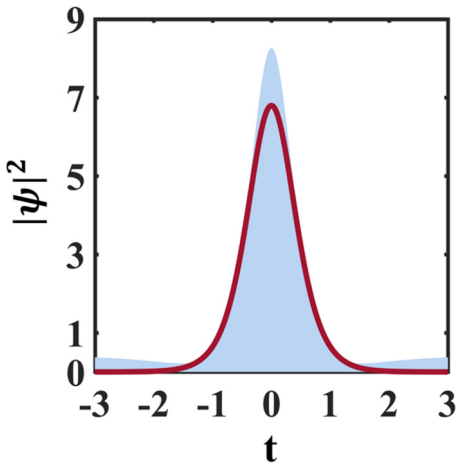

FIG. 2. Comparison of the actual CS (shaded) and the ansatz (solid line) used in the variational formulation.

$$L = \frac{i}{2}(\psi\psi_\tau^* - \psi_\tau\psi^*) + |\psi_t|^2 - \frac{1}{2}|\psi|^4 + \sigma|\psi|^2, \tag{6}$$

$$R = i(\psi\psi_\tau^* - \psi_\tau\psi^*) + i(E_{in}^*\psi_\tau - E_{in}\psi_\tau^*). \tag{7}$$

It is observed that even a small value of modulation depth ($M \ll 1$) can influence the trajectory of the CS. Therefore, we approximate E_{in} as mentioned in Eq. (4) as

$$E_{in}(t) \approx P_{in}[1 + iM\cos(\omega t)] \approx P_{in}\left(1 + iM - \frac{iM\omega^2 t^2}{2}\right). \tag{8}$$

Exploiting the EL equation with the help of a reduced form of the Lagrangian ($L_g = \int_{-\infty}^{\infty} L\,dt$) and RDF ($R_g = \int_{-\infty}^{\infty} R\,dt$) (see the derived forms of L_g and R_g in Appendix A), we derive a set of coupled ordinary differential equations (ODEs) describing the overall soliton dynamics (η, δ, ϕ, t_p). The equations of motion for individual pulse parameters are as follows:

$$\frac{\partial\eta}{\partial\tau} = -4\eta + \frac{\sqrt{\eta}}{2}\left(2\sqrt{2}\pi P_{in} - \frac{\pi^3\delta^2 P_{in}}{2\sqrt{2}\eta}\right)(\cos\phi + M\times\sin\phi) - \frac{M\omega^2\sqrt{\eta}}{4}\left[2\sqrt{2}P_{in}\sin\phi\left(\frac{\pi^3}{4\eta} + \pi t_p^2\right) - \frac{2\delta^2 P_{in}}{\eta}\right.$$
$$\left.\times\sin\phi\left(\frac{\pi^3 t_0^2}{4} + \frac{5\pi^5}{16\eta}\right) - \frac{\sqrt{2}\delta\pi^3 P_{in}t_p\cos\phi}{\eta} + \frac{5\sqrt{2}\pi^5\delta^3 P_{in}}{24\eta^2}\times t_p\cos\phi\right], \tag{9}$$

$$\frac{\partial\phi}{\partial\tau} = -\sigma + \eta + \delta^2 + \frac{\pi^3 P_{in}\delta^2}{2\sqrt{2}\eta^{3/2}}(\sin\phi + M\cos\phi) + \frac{5\sqrt{2}M\omega^2\pi^3\delta P_{in}t_p\sin\phi}{8\eta^{3/2}} - \frac{5\pi^5\delta^4 P_{in}M\cos\phi}{96\sqrt{2}\eta^{3/2}}$$
$$- \frac{55\sqrt{2}\delta^2 P_{in}t_p\pi^5 M\omega^2\sin\phi}{192\eta^{3/2}} - \frac{M\omega^2 P_{in}\delta^4\cos\phi}{12\sqrt{2}\eta^{3/2}}\left(\frac{61\pi^7}{64\eta} + \frac{5\pi^5 t_p^2}{16}\right) - \frac{M\omega^2 P_{in}\delta^2\cos\phi\pi^3}{8\eta^{3/2}}\left(\frac{25\sqrt{2}\pi^2}{8\eta} + \frac{3t_p^2}{\sqrt{2}}\right), \quad (10)$$

$$\frac{\partial\delta}{\partial\tau} = -\frac{\delta}{4\sqrt{\eta}}\left(2\sqrt{2}\pi P_{in} - \frac{\pi^3\delta^2 P_{in}}{2\sqrt{2}\eta}\right)(\cos\phi + M\sin\phi) + \frac{M\omega^2}{4\sqrt{\eta}}\left[2\sqrt{2}\pi P_{in}t_p\cos\phi + \sqrt{2}\delta P_{in}\pi t_p^2\sin\phi\right.$$
$$\left.\times\left(1 - \frac{\delta^2\pi^2}{4\sqrt{2}\eta}\right) + \frac{3\delta P_{in}\pi^3\sin\phi}{2\sqrt{2}\eta} - \frac{\sqrt{2}\pi^3\delta^2 P_{in}t_p\cos\phi}{\eta} \times \left(1 + \frac{5\pi^2}{96\eta}\right)\right], \quad (11)$$

$$\frac{\partial t_p}{\partial\tau} = -2\delta + \frac{\delta P_{in}\pi^3}{4\sqrt{2}\eta^{3/2}}(\sin\phi - M\cos\phi) - \frac{M\omega^2}{4\sqrt{2}\eta^3} \times \left[P_{in}t_p\pi^3\sin\phi - 2\sqrt{2}\delta P_{in}\cos\phi\left(\frac{5\pi^5}{16\eta} + \frac{\pi^3 t_p^2}{4}\right)\right.$$
$$\left. - \frac{5\pi^5\delta^2 P_{in}t_p\sin\phi}{8\sqrt{2}\eta} + \frac{P_{in}\delta^3\cos\phi}{3\sqrt{2}\eta}\left(\frac{61\pi^7}{64\eta} + \frac{5\pi^5 t_p^2}{16}\right)\right]. \quad (12)$$

To obtain closed-form expressions for the CS trajectory as well as the peak amplitude and phase of the generated CS in the steady state, we found that the contributions of those terms containing higher orders of δ ($\delta^n, n \geqslant 2$) in Eqs. (9)–(12) are negligible.

B. Prediction of the soliton trajectory

From the mathematical expressions Eqs. (9)–(12), it is evident that pulse parameters undergo some changes during propagation for nonvanishing M. In Fig. 3(a), we plot the trajectory of a CS under a phase-modulated external pump. We observe that the CS acquires a drift velocity during its propagation. The trajectory of the soliton is influenced by the modulation depth. The numerical solution of the coupled ODEs predicts the trajectory nicely [see Fig. 3(b)]. However, those ODEs will be more useful if we decouple them with suitable approximations(see Appendix B). It can be shown that the dynamic expression for the temporal shift of the pulse is

$$t_p(\tau) \approx t_p(0)\exp(-2M\omega^2\tau). \quad (13)$$

Equation (13) clearly indicates with an increase in slow time (τ), the location of the pulse shifts toward the origin ($t = 0$). Here modulation depth (M) and modulation frequency (ω) act as parameters and control the drift velocity of the generated CS. The pulse shifts to its stationary location at less round trips with increasing M or ω [see Figs. 3(c) and 3(d)]. The drift velocity has been previously mentioned to be directly proportional to the gradient of the external driving field [26,35]. Our calculations enable us to obtain a simple mathematical form for the drift velocity of the generated CS, which is given as $v_d(\tau) = \frac{dt_p}{d\tau} \approx -2M\omega^2 t_p(\tau)$. In Fig. 4 we observe that drift velocity of the CS initially increases and gradually saturates to null value and thus the CS obtains its stationary position.

The behavior of the CS trajectory can be understood in an alternative way with the concept of intracavity field momentum, which is defined by [11]

$$P = -\frac{i}{2}\int_{-\infty}^{\infty}\left(\psi^*\frac{d\psi}{dt} - \psi\frac{d\psi^*}{dt}\right)dt. \quad (14)$$

Using this definition along with Eq. (2), the rate of change of momentum of the intracavity field is found to be

$$\frac{dP}{d\tau} = -2P - \mathrm{Im}\int_{-\infty}^{\infty}\psi\frac{dE_{in}^*}{dt}\,dt. \quad (15)$$

In the absence of any modulation (phase or amplitude) of the pump, the rate of change of momentum is determined only by the first term of the right-hand side of Eq. (15) and the momentum seems to decay exponentially with $\tau \to \infty$ such that the net force acting on the soliton also vanishes

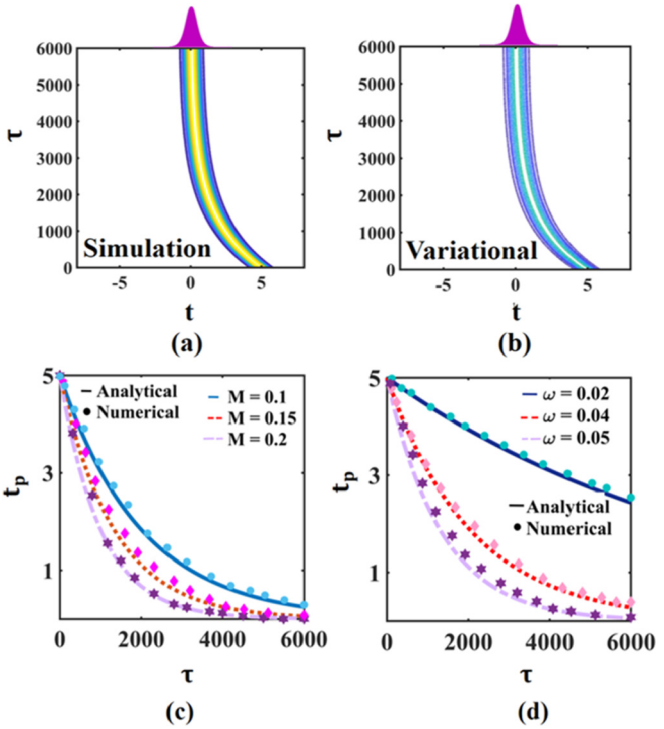

FIG. 3. Contour plots of (a) simulation and (b) variational results showing the trajectory of the CS under the influence of a phase-modulated driving field. (c) Variation of the CS trajectory with different phase-modulation depth (M) and (d) different phase-modulation frequency (ω) of cw, shown both numerically and analytically.

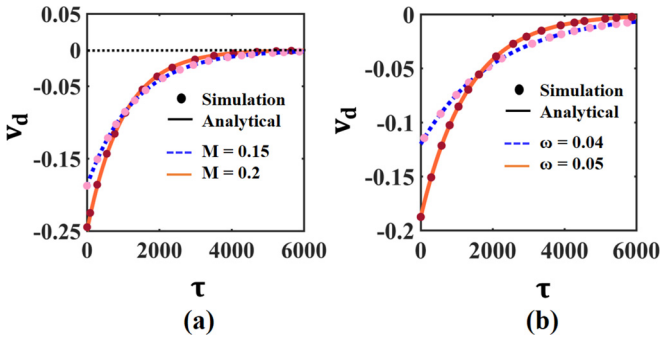

FIG. 4. Drift velocity (v_d) profile of the CS shown both numerically and analytically. (a) Variation of drift velocity with propagation for two modulation depths [$M = 0.15$ (dotted), $M = 0.2$ (solid)]. (b) Drift velocity profile for two modulation frequencies [$\omega = 0.04$ (dotted), $\omega = 0.05$ (solid)].

with propagation and the soliton eventually acquires its steady position. Note that in this problem the phase of the driving field is modulated as $\phi(t) = M\chi(t) = M\cos(\omega t)$. In the presence of phase modulation (i.e., $E_{in} = P_{in}e^{\phi(t)}$) the second term of the Eq. (15), which contains the gradient of the driving field, will dominate. Now, the CS will gradually acquire its stationary position where the gradient of the driving field, i.e., dE_{in}/dt (or $\frac{d\phi}{dt}$), vanishes. Note that ψ and E_{in} both are in general complex with a phase term. Since the amplitude of ψ (which represents soliton) is a symmetric function, it is easy to show that the integrand in Eq. (15) vanishes when $\frac{d\phi}{dt}$ is an asymmetric function or zero. Now when the function $\frac{d\phi}{dt}$ is neither symmetric nor asymmetric the integrand can still vanish, if $\frac{d\phi}{dt} = 0$ and the soliton is dragged to that point. We illustrate this phenomenon in Fig. 5 where the soliton is dragged at the point where dE_{in}/dt (or $\frac{d\phi}{dt}$) vanishes. Note that the concept of the intracavity field momentum only locates the stabilized temporal position of an off-shifted CS under a phase-modulated pump. It can never predict the pulse trajectory like variational treatment does. The variational treatment can be extended further to evaluate the other pulse parameters such as amplitude ($A = \sqrt{2\eta}$), phase (ϕ), and frequency shift (δ). In Fig. 6 we plot the variation of A, ϕ, and δ as a function of slow time (τ). We know the dissipative CSs always emerge out of the cw background unlike the Kerr solitons in

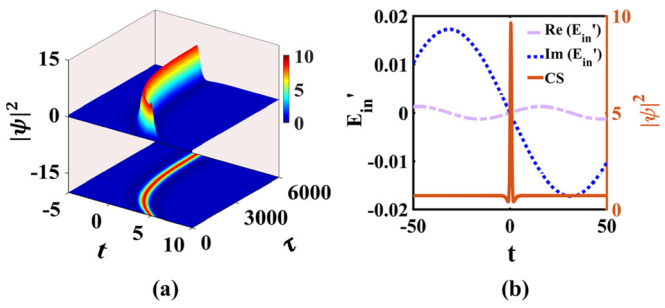

FIG. 5. (a) CS undergoes a shift in its reference frame due to a phase-modulated cw pump ($E_{in} = P_{in}e^{\phi(t)}$). (b) Left axis: gradient of external pump field $\frac{dE_{in}}{dt} = E'_{in}$; right axis: final steady position of the generated CS.

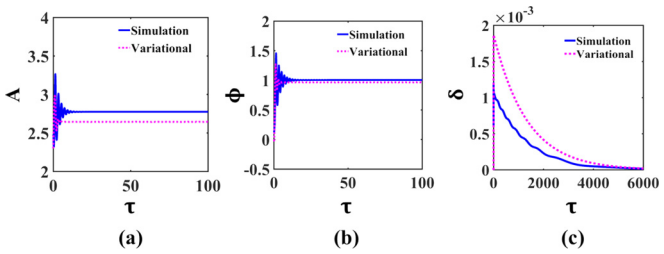

FIG. 6. Evolution of CS parameters under a phase-modulated driving field shown both numerically and with variational analysis. (a) Amplitude ($A = \sqrt{2\eta}$), (b) phase (ϕ), and (c) frequency shift (δ).

the conservative system. During our variational analysis we assume a sech pulse shape which is merely an approximation. Note, in order to get rid of the homogeneous pedestal (ψ_h), we rescale the field as $|\psi(t,\tau)|^2 \to |\psi(t,\tau)|^2 - |\psi_h|^2$ and compare it with variational result in Fig. 6. It is observed that the variational results are in good agreement with the results obtained from full numerical solution of the LLE.

C. Derivation of the stationary solution

By exploiting the variational expressions we extract the steady-state condition for the CS. Without any phase modulation ($M = 0$), from Eqs. (9) and (10), we obtain the amplitude and phase of the CS in its steady state as

$$\eta = \sigma, \qquad \phi = \cos^{-1}\left(\frac{2\sqrt{2\eta}}{\pi P_{in}}\right) = \cos^{-1}\left(\frac{2\sqrt{2\sigma}}{\pi P_{in}}\right). \tag{16}$$

From Eq. (16) it is evident that for a given pump power (P_{in}) the CS ceases to exist when $\sigma > \frac{\pi^2 P_{in}^2}{8}$. We numerically verify this argument by keeping $P_{in} = 2.3$ and find that the CS is generated when $\sigma \leqslant 6.5$, which is consistent with the expression we have derived. In a phase-space diagram, the CS always makes a spiral [12] centered about a point known as the fixed point of the system. This spiral nature is a signature of the evolution of amplitude and phase of the generated CS. Under phase modulation, the fixed point might change as depicted in Fig. 7(a). For nonvanishing M, Eq. (16) is

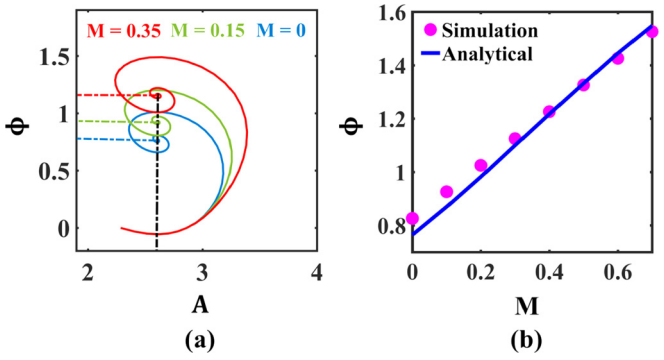

FIG. 7. (a) Phase-space diagram of the generated CS in three different cases, without modulation (M), $M = 0.15$, and $M = 0.35$, respectively. (b) Variation of soliton phase (ϕ) with modulation depth (M); shown for both numerical and analytical results.

modified as

$$\eta \approx \sigma,$$
$$\phi \approx \tan^{-1}M + \cos^{-1}\left(\frac{B}{\sqrt{1+M^2}}\right), \tag{17}$$

where $B = \frac{2\sqrt{2\sigma}}{\pi P_{in}}$. In Fig. 7(b), we plot the CS phase (ϕ) as a function of modulation depth (M). We observe that the variational results (solid line) agree well with the full numerical results (filled circles).

IV. SOLITON INTERACTION IN THE PRESENCE OF A CONSTANT DRIVING FIELD

The earlier work of Malomed and Akhmediev and later several other authors have considered the detailed analysis of the soliton (bright-bright, bright-dark) interaction problem in a conservative system [36–42]. The stability of two- and multisoliton states has also been reported for dissipative solitons where the system contains a gain medium [43–45], or in a coherently driven passive microresonator [22,31,46,47]. In recent papers [30,31], soliton interaction and the possibility of the formation of BS in a microresonator system has been studied thoroughly. For normalized detuning value $\sigma < 2$, the generated CS has an oscillatory tail, such that a second soliton can lock at any extrema of the tail oscillations. One can find the stable and unstable equilibrium separation by calculating the interaction potential [30,37]. On the other hand, for higher detuning value the CS tail becomes monotonous, and oscillations become too weak to form any BS, which is the case we consider here. We encountered three different situations likely: attraction, repulsion, or independent soliton propagation depending on the initial delay between two CSs. Our reduced analytical model can predict these results quite well. To visualize the overall dynamics of two copropagating CSs, we numerically solve Eq. (2) with the initial wave function of the form $\psi(0,t) = \sqrt{2\sigma}\,\mathrm{sech}[\sqrt{\sigma}(t-t_p)] + \sqrt{2\sigma}\,\mathrm{sech}[\sqrt{\sigma}(t+t_p)]$. We consider zero phase modulation ($M = 0$) such that E_{in} becomes P_{in} in Eq. (2). The simulation is performed with the constant values of $\sigma = 3.4$ and $P_{in} = 2.3$ and in each case we vary the initial separation ($2t_p$) between two CSs.

A. Derivation of the reduced model

We find that the well-known variational treatment beautifully brings out the variation of the soliton parameters such as amplitude, phase, and frequency shift during different interaction scenarios. We assume soliton 1 (ψ_1) propagates in such a way that only the tail of soliton 2 (ψ_2) interacts with it. The governing equation of soliton 1 is [18]

$$i\frac{\partial\psi_1}{\partial\tau} + \frac{\partial^2\psi_1}{\partial t^2} + |\psi_1|^2\psi_1 + 2|\psi_1|^2\psi_2 + \psi_1^2\psi_2^* - \sigma\psi_1 + i\psi_1 - iP_{in} = 0. \tag{18}$$

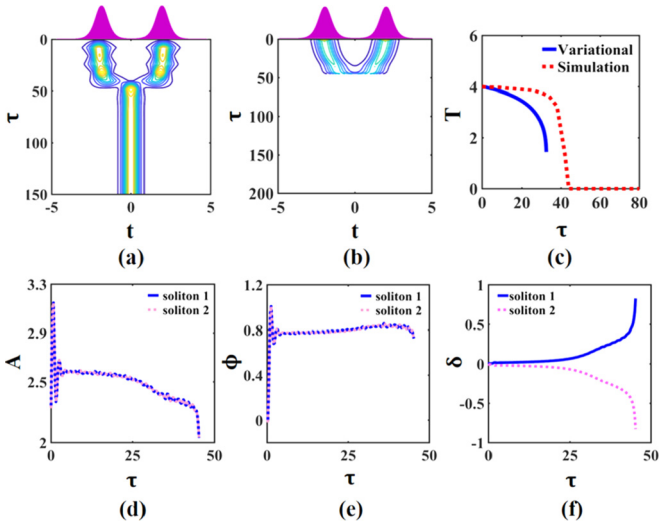

FIG. 8. Evolution of two CSs when initial separation $2t_p = 4$. First row: Path of the soliton shown with both (a) numerical and (b) variational results. (c) Separation ($2t_p = T$) between two solitons with propagation. Second row: Analytical model showing the evolution of two-soliton parameters: (d) amplitude, (e) phase, and (f) frequency shift.

The Lagrangian and the RDF correspondingly are written as

$$L = \frac{i}{2}(\psi_1\psi_{1\tau}^* - \psi_{1\tau}\psi_1^*) + |\psi_{1t}|^2 - \frac{1}{2}|\psi_1|^4 + \sigma|\psi_1|^2, \tag{19}$$

$$R = (2|\psi_1|^2\psi_2 + \psi_1^2\psi_2^*)\psi_{1\tau}^* + (2|\psi_1|^2\psi_2^* + \psi_1^{*2}\psi_2)\psi_{1\tau} + i(\psi_1\psi_{1\tau}^* - \psi_{1\tau}\psi_1^*) - iP_{in}(\psi_{1\tau}^* - \psi_{1\tau}). \tag{20}$$

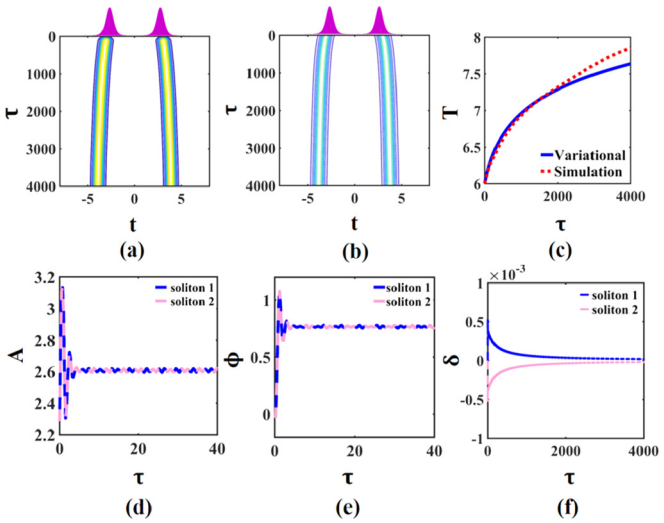

FIG. 9. Evolution of two CSs when the initial separation $2t_p = 6$. First row: Path of the soliton showing both (a) numerical and (b) variational results. (c) Separation ($2t_p = T$) between two solitons with propagation. Second row: Analytical model showing the evolution of two-soliton parameters: (d) amplitude (e) phase, and (f) frequency shift.

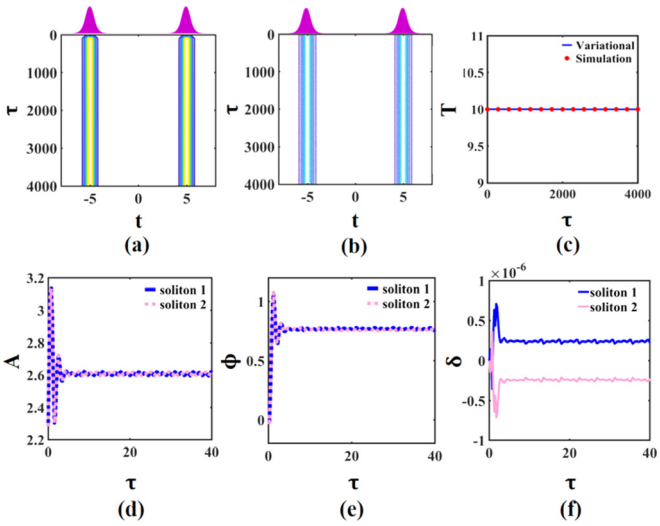

FIG. 10. First row: Independent propagation of two CSs when the initial separation $2t_p = 10$. (a) Numerical result and (b) variational result. (c) Separation ($2t_p = T$) between two solitons with propagation. Second row: Analytical model showing the evolution of two-soliton parameters: (d) amplitude, (e) phase, and (f) frequency shift.

The derived forms of the Lagrangian and RDF density using the ansatz function for soliton 1 are given in Appendix C. The evolution equations for soliton 1 (ψ_1) are

$$\frac{\partial \eta_1}{\partial \tau} = -4\eta_1 + 16\eta_1\sqrt{\eta_1\eta_2}e^{-\sqrt{\eta_1}T}\sin\theta + \sqrt{2\eta_1}\pi P_{in}\cos\phi_1 - \frac{\pi^3\delta_1^2 P_{in}\cos\phi_1}{4\sqrt{2\eta_1}}, \tag{21}$$

$$\frac{\partial \delta_1}{\partial \tau} = 8\eta_1\sqrt{\eta_2}\cos\theta e^{-\sqrt{\eta_1}T} - \left(1 - \frac{\pi^2\delta_1^2}{8\eta_1}\right) \times \frac{\delta_1\cos\phi_1\pi P_{in}}{\sqrt{2\eta_1}}, \tag{22}$$

$$\frac{\partial t_1}{\partial \tau} = -2\delta_1 - 4\sqrt{\eta_2}\sin\theta e^{-\sqrt{\eta_1}T} + \left(1 - \frac{5\pi^2\delta_1^2}{24\eta_1}\right) \times \frac{\pi^3\delta_1 P_{in}\sin\phi_1}{4\sqrt{2}\eta_1^{3/2}}, \tag{23}$$

$$\frac{\partial \phi_1}{\partial \tau} = -\sigma + \delta_1^2 + \eta_1 + 12\sqrt{\eta_1\eta_2}\cos\theta e^{-\sqrt{\eta_1}T} + 4\delta_1\sqrt{\eta_2} \times \sin\theta e^{-\sqrt{\eta_1}T} - \frac{\pi^3 P_{in}\delta_1^2\sin\phi_1}{2(2\eta_1)^{3/2}}\left(2 - \frac{5\pi^2\delta_1^2}{24\eta_1}\right), \tag{24}$$

where $\theta = \phi_1 - \phi_2$ and $T = t_1 - t_2$.

In a similar way one can also find out the evolution equations for soliton 2 (ψ_2) parameters as follows:

$$\frac{\partial \eta_2}{\partial \tau} = -4\eta_2 - 16\eta_2\sqrt{\eta_1\eta_2}e^{-\sqrt{\eta_2}T}\sin\theta + \sqrt{2\eta_2}\pi P_{in} \times \cos\phi_2 - \frac{\pi^3\delta_2^2 P_{in}\cos\phi_2}{4\sqrt{2\eta_2}}, \tag{25}$$

$$\frac{\partial \delta_2}{\partial \tau} = -8\eta_2\sqrt{\eta_1}\cos\theta e^{-\sqrt{\eta_2}T} - \left(1 - \frac{\pi^2\delta_2^2}{8\eta_2}\right) \times \frac{\delta_2\cos\phi_2\pi P_{in}}{\sqrt{2\eta_2}}, \tag{26}$$

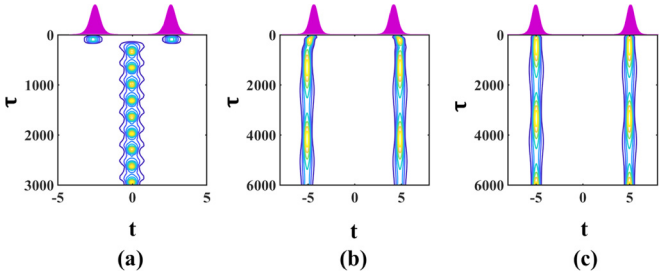

FIG. 11. Contour plot showing the CS breathing state for $[\sigma, P_{in}] = [4.2, 3]$. (a) Attraction state $[2t_p = 4]$. (b) Repulsion state $[2t_p = 6]$. (c) Independent soliton state $[2t_p = 10]$.

$$\frac{\partial t_2}{\partial \tau} = -2\delta_2 - 4\sqrt{\eta_1}\sin\theta e^{-\sqrt{\eta_2}T} + \left(1 - \frac{5\pi^2\delta_2^2}{24\eta_2}\right) \times \frac{\pi^3\delta_2 P_{in}\sin\phi_2}{4\sqrt{2}\eta_2^{3/2}}, \tag{27}$$

$$\frac{\partial \phi_2}{\partial \tau} = -\sigma + \delta_2^2 + \eta_2 + 12\sqrt{\eta_1\eta_2}\cos\theta e^{-\sqrt{\eta_2}T} + 4\delta_2\sqrt{\eta_1}\sin\theta e^{-\sqrt{\eta_2}T} - \frac{\pi^3 P_{in}\delta_2^2\sin\phi_2}{2(2\eta_2)^{3/2}}\left(2 - \frac{5\pi^2\delta_2^2}{24\eta_2}\right). \tag{28}$$

A set of eight coupled ordinary differential equations (21)–(28) describe the overall dynamics of two copropagating CSs. It is observed that the initial separation between CSs controls the strength of the interaction and based on which three distinct situations arise: attraction, repulsion, and independent soliton propagation. In Fig. 8, we show how two copropagating CSs attract themselves to form a single state. A detailed variational treatment predicts identical behavior [see plot in Fig. 8(c)] and locates the collision point from where the single soliton emerges. Combining Eqs. (22),(23) and Eqs. (26),(27) we derive a second-order differential equation which approximately predicts the variation of two-soliton

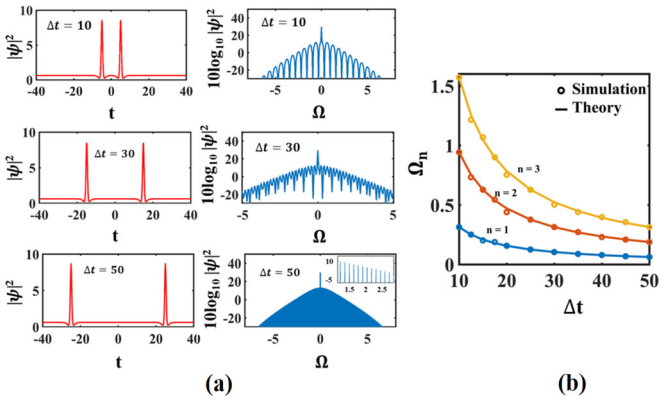

FIG. 12. (a) Effect of the CS interaction on the generated frequency comb; interference fringe density changes with separation or delay (Δt) between the two CSs. (b) Position of interference fringes of different order vs. delay (Δt) between two CSs.

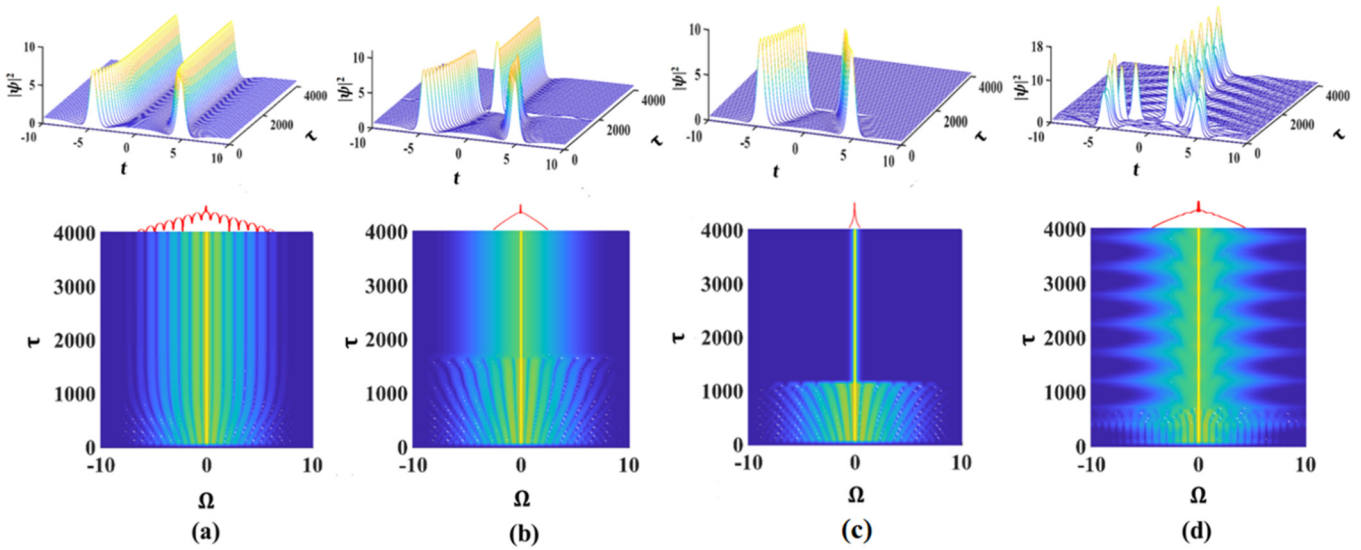

FIG. 13. Dynamics of soliton interaction in the presence of cosine-modulated phase profile ($M = 0.15$) of the driving field when the mutual separation $2t_p = 10$ and modulation frequency $\omega = 0.05$. (a) $[\sigma, P_{in}] = [2.9, 2]$ two-soliton state, (b) $[\sigma, P_{in}] = [3.4, 2.3]$ merged CSs, (c) $[\sigma, P_{in}] = [4, 2.2]$ annihilated CSs, and (d) $[\sigma, P_{in}] = [4.2, 3]$ merged breathing CSs.

separation ($T = t_1 - t_2$) given as

$$\frac{\partial^2 T}{\partial \tau^2} + B\frac{\partial T}{\partial \tau} \approx 2A(C-2)e^{-\sqrt{\eta}T}. \tag{29}$$

In order to derive this differential equation, we have assumed $\eta_1 = \eta_2 = \eta$ and $\phi_1 = \phi_2 = \phi$. The constants in the equations are as follows: $A = 8\eta^{3/2}\cos\theta$, $B = \frac{\pi\cos\phi P_{in}}{\sqrt{2\eta}}$, $C = \frac{\pi^3 \sin\phi P_{in}}{(2\eta)^{3/2}}$. Note that a variational analysis is applicable whenever two independent solitons exist. It will not produce any results when two solitons merge to form a single soliton because for such case, the assumption of ansatz function is violated. However, variational results work nicely before collision and we find the evolution of A, ϕ, and δ in Figs. 8(d)–8(f). A further increase in separation will lead to repulsion (see Fig. 9) and independent propagation of two CSs (see Fig. 10). We study all three cases based on the variational results. Note that in all three cases the frequency shift for an individual soliton is nonidentical (in fact, opposite in magnitude) and results in three different dynamics. In a special situation depending upon the external parameters (σ, P_{in}), we obtain a steady breather CS where the peak power of the CS periodically breathes over round-trip evolution. Like previous situations, a different initial delay between two pulses led to attractive or repulsive force or the creation of two independent breather CSs (see Fig. 11).

B. Soliton interaction mediated frequency comb generation

It is well known that CS corresponds to a frequency comb in spectral domain with single FSR spacing. Due to four-wave mixing and proper phase matching, side modes are excited from the resonant pump mode of the cavity. On the other hand, for the soliton interaction problem, we can intuitively say that two resonant modes are simultaneously excited which interfere. By solving the LLE, we observe interference fringes in the frequency spectrum. Such interference fringes with high contrast reflect stable binding separation [48]. Here, we choose a different time delay between the two CSs where they can propagate independently. Interference patterns are changed with their binding separation. The position of the individual interference maxima changes with the separation [see Fig. 12(a)]. The interference pattern becomes denser with increasing binding separation. For a fixed delay, the interference maximas locate at

$$\Omega_n = \pm\left(n - \tfrac{1}{2}\right)\Delta\Omega, \tag{30}$$

where $n = 1, 2, 3, \ldots$ and $\Delta\Omega = 2\pi/\Delta t$. n is the interference maxima order and Ω_n are the corresponding frequencies. In Fig. 12(b) we observe that our simulation results agree quite well with the analytical formulas.

V. SOLITON INTERACTION IN PRESENCE OF PHASE-MODULATED DRIVING FIELD

Finally, we consider a copropagating soliton interaction when the driving beam is phase modulated with a cosine profile at a frequency ω with modulation depth M. To illustrate the interaction mechanism, we numerically integrate Eq. (2) using a symmetric initial condition $\psi(0,t) = \sqrt{2\sigma}\{\mathrm{sech}[\sqrt{\sigma}(t - t_p)] + \mathrm{sech}[\sqrt{\sigma}(t + t_p)]\}$. The initial separation ($2t_p = 10$) is made larger compared to the characteristic width of the CS in order to avoid any self-interaction during propagation. This ensures that two CSs can move independently in the absence of any modulated driving field. We observe different interaction scenarios based on two external parameters: cavity detuning frequency (σ) and pump power (P_{in}).

In Fig. 13, we show the evolution of two copropagating CSs for four different sets of (σ, P_{in}). We observe that depending on the external parameters (σ, P_{in}) four distinct states may evolve: (a) a stationary two-soliton state, (b) a single soliton state after merging, (c) an annihilation state, and finally (d) a breathing state. The spectral evolution is also plotted for four

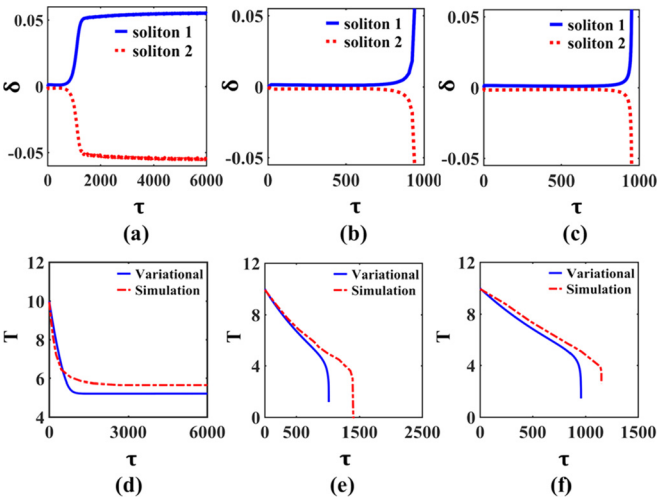

FIG. 14. First row: Variation of frequency shift (variational results). Second row: Variation of separation of two CSs when modulation depth $M = 0.15$. (a) and (d) Two-soliton state $[\sigma, P_{in}] = [2.9, 2]$. (b) and (e) Merged state $[\sigma, P_{in}] = [3.4, 2.3]$. (c) and (f) Annihilated state $[\sigma, P_{in}] = [4, 2.2]$.

different cases. As expected, interference fringes are observed for the two-soliton state, whereas an annihilated state exhibits a single frequency complimenting the cw background in time domain. For the single-soliton state and the breathing state the spectra are almost identical.

A. Analysis of the reduced model

The variational analysis discussed in earlier sections (Secs. III and IV) are useful here to visualize the pulse dynamics in this complex scenario. In Fig. 14 we observe that the different final stationary states such as the two-soliton state, merged single-soliton state or annihilated state corresponds to different frequency shifts. Though the variational formalism cannot capture the single-soliton state after merging, it can well predict the point of merging and annihilation of two CSs. The evolution equations of the two soliton parameters are mentioned in Appendix D. We adopt the variational results (solid lines) to obtain the separation (T) as a function of slow time (τ) and find a close agreement with full numerical analysis (dotted lines). In Fig. 15(a), we plot τ_c as a function of M for a fixed ω for both the merged single-soliton state and the annihilated state. For a given set of (σ, P_{in}), the collision point (τ_c) changes with the values of modulation depth (M). The solitons collide earlier for larger M. The simulated values are given by filled circles whereas the solid line depicts the variational result. The variational analysis compliments the numerical results with a certain degree of accuracy. The CS which contains a pedestal is approximated as a sech shape in variational treatment and perhaps this is the reason why we have the mismatch of two results at lower modulation depth (M). So, it is evident that the parameter set (σ, P_{in}) leads to a different steady state of the intracavity field whereas the parameter set (M, ω) mainly controls the drift velocity of the generated CSs.

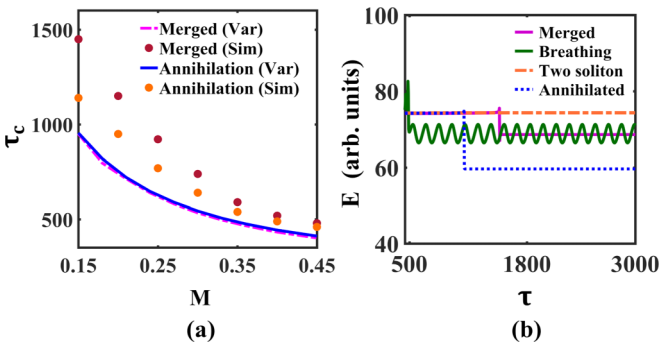

FIG. 15. (a) Variation of the collision distance (τ_c) with modulation depth (M), shown both with simulation and variational results for the merged and annihilated state (b) Numerically simulated intracavity field energy (E) evolution for all the four (two soliton state, merged, annihilation and breathing) cases.

B. Intracavity field energy

Finally, we compare the relative intracavity field energy for four cases in Fig. 15(b) by numerically computing the quantity $E = \int_{-t_{\min}}^{t_{\max}} \psi^* \psi \, dt$ over the slow time. We observe that the total energy remains almost steady throughout the evolution time for the stationary two-soliton state. For merged and annihilated states the energy drops sharply at some critical τ corresponding to the point of merging or annihilation. During annihilation, the energy does not drop to zero as the resonator always has the constant cw field, which is clearly visible in the temporal dynamics of annihilation in Fig. 13(c). For the breathing state we observe oscillatory energy. The mean energy of oscillation for the breathing soliton is found to be identical to the final energy of the merged single soliton.

VI. CONCLUSION

We have studied the complex dynamics of a single CS and copropagating CSs separately in a passive fiber loop resonator under a phase-modulated driving field. A semianalytical variational method is adopted to unfold the unique behavior of temporal CSs under this driving field. The variational calculations led to an in-depth analysis for each perturbation situation and results in obtaining a set of ordinary differential equations which determine the evolution of individual pulse parameters. We start with a single soliton whose temporal trajectory is controlled by the modulation depth and the modulation frequency of the external pump. The variational analysis efficiently predicts the path followed by the CS. The derived explicit form of the temporal trajectory and the drift velocity of CSs will enable us to control them externally with the modulation parameters. The phase-space diagram portrays the amplitude and phase evolution of CSs under this perturbation. During the two-soliton interaction, this semianalytical treatment can efficiently find out the role of different external parameters such as delay, detuning frequency, pump power, modulation depth, and modulation frequency which can enrich any numerical and experimental results. We believe that our analysis will help one to investigate single or multiple CS dynamics further in the presence of several other forms of phase- or amplitude-modulated external fields.

ACKNOWLEDGMENTS

M.S. would like to thank Ministry of Human Resource Development, Government of India and IIT Kharagpur for funding to carry out her research work.

APPENDIX A: DERIVATIONS OF THE REDUCED LAGRANGIAN AND RDF FOR THE CASE MENTIONED IN SEC. III

To obtain the set of coupled differential equations for the evolution of CS parameters, these steps are followed.

Step 1. The ansatz function:

$$\psi(t,\tau) = \sqrt{2\eta(\tau)}\,\mathrm{sech}\{\sqrt{\eta(\tau)}[t - t_p(\tau)]\} \times \exp(i\{\phi(\tau) - \delta(\tau)[t - t_p(\tau)]\}). \quad \text{(A1)}$$

The driving field is

$$E_{in}(t) \approx P_{in}[1 + iM\cos(\omega t)] \approx P_{in}\left(1 + iM - \frac{iM\omega^2 t^2}{2}\right). \quad \text{(A2)}$$

The explicit form of the Euler-Lagrangian (EL) equation is

$$\frac{d}{d\tau}\left(\frac{\partial L}{\partial \psi_\tau^*}\right) + \frac{d}{dt}\left(\frac{\partial L}{\partial \psi_t^*}\right) - \frac{\partial L}{\partial \psi^*} + \left(\frac{\partial R}{\partial \psi_\tau^*}\right) = 0. \quad \text{(A3)}$$

We choose the form of Lagrangian (L) and RDF (R) function intuitively in such a way that the above EL equation will give back the original form of the LLE $\frac{\partial\psi}{\partial\tau} = -(1+i\sigma)\psi + i|\psi|^2\psi + i\frac{\partial^2\psi}{\partial t^2} + E_{in}$:

$$L = \frac{i}{2}(\psi\psi_\tau^* - \psi_\tau\psi^*) + |\psi_t|^2 - \frac{1}{2}|\psi|^4 + \sigma|\psi|^2, \quad \text{(A4)}$$

$$R = i(\psi\psi_\tau^* - \psi_\tau\psi^*) + i(E_{in}^*\psi_\tau - E_{in}\psi_\tau^*). \quad \text{(A5)}$$

Step 2. Now we integrate the Lagrangian and Rayleigh's function over the fast time (t):

$$L_g = \int_{-\infty}^{\infty} L\,dt, \quad \text{(A6)}$$

$$R_g = \int_{-\infty}^{\infty} R\,dt. \quad \text{(A7)}$$

The forms of (L_g) and RDF (R_g) are as follows:

$$L_g = 4\sqrt{\eta}\left(\delta\frac{\partial t}{\partial\tau} + \frac{\partial\phi}{\partial\tau} - \frac{\eta}{3} + \sigma + \delta^2\right), \quad \text{(A8)}$$

$$\begin{aligned}
R_g = {} & 8\sqrt{\eta}\left(\delta\frac{\partial t_p}{\partial\tau} + \frac{\partial\phi}{\partial\tau}\right) - \frac{\partial\eta}{\partial\tau}\frac{\pi^3 P_{in}\delta^2}{\sqrt{2}\eta^2}(\sin\phi - M\cos\phi) + 2\sqrt{2}P_{in}\pi\delta\frac{\partial t_p}{\partial\tau}\left(1 - \frac{\pi^2\delta^2}{8\eta}\right)(\cos\phi + M\sin\phi) \\
& - \left(\delta P_{in}\frac{\partial t_p}{\partial\tau} + P_{in}\frac{\partial\phi}{\partial\tau}\right)\left[(\cos\phi + M\sin\phi)\left(2\sqrt{2}\pi - \frac{\pi^3\delta^2}{2\sqrt{2}\eta}\right)\right] + \frac{\delta P_{in}\pi^3}{\sqrt{2}\eta}\left(1 - \frac{5\pi^2\delta^2}{24\eta}\right)\frac{\partial\delta}{\partial\tau}(\sin\phi - M\cos\phi) \\
& - \frac{M\omega^2}{2}\left\{\left(-\frac{\partial\eta}{\partial\tau}\times\frac{2P_{in}\pi^3}{\eta^2}\right)\left(\cos\phi + \sqrt{2}\delta t_p\sin\phi - \frac{5\sqrt{2}\delta^2\pi^2\cos\phi}{8\eta} - \frac{P_{in}\delta^2 t_p^2\cos\phi}{2\sqrt{2}} - \frac{\delta^3\pi^2 t_p\sin\phi}{6\sqrt{2}\eta}\right)\right. \\
& + \frac{\partial t_p}{\partial\tau}\left[4\sqrt{2}\pi P_{in}t_p\cos\phi\left(1 - \frac{\pi^2\delta^2}{4\eta} - \frac{5\pi^4\delta^4}{96\eta^2}\right) + \frac{\sqrt{2}\pi^3\delta P_{in}\sin\phi}{\eta} - \frac{5\delta^3\sin\phi P_{in}\pi^5}{\sqrt{2}\eta^2}\right] - \frac{\partial\phi}{\partial\tau}\left[2\sqrt{2}P_{in}\sin\phi\left(\frac{\pi^3}{4\eta} + \pi t_p^2\right)\right. \\
& \left. - \sqrt{2}\delta^2 P_{in}\sin\phi\left(\frac{\pi^3 t_p^2}{4\eta} + \frac{5\pi^5}{16\eta^2}\right) - \frac{\sqrt{2}P_{in}t_p\pi^3\delta\cos\phi}{\eta} + \frac{5\sqrt{2}\pi^5\delta^3 P_{in}t_p\cos\phi}{24\eta^2}\right] + \frac{\partial\delta}{\partial\tau}\times\left[\frac{\sqrt{2}P_{in}t_p\pi^3}{\eta}\sin\phi\left(1 - \frac{5\delta^2\pi^2}{4\sqrt{2}\eta}\right)\right. \\
& \left.\left. - 2\sqrt{2}P_{in}\delta\cos\phi\left(\frac{5\pi^5}{16\eta^2} + \frac{\pi^3 t_p^2}{4\eta}\right) + \frac{\sqrt{2}P_{in}\delta^3\cos\phi}{3\eta^2}\left(\frac{61\pi^7}{64\eta} + \frac{5\pi^5 t_p^2}{16}\right)\right]\right\}. \quad \text{(A9)}
\end{aligned}$$

Step 3. Now using the form of L_g and R_g in

$$\frac{d}{d\tau}\left(\frac{\partial L_g}{\partial\dot{p}_j}\right) - \frac{\partial L_g}{\partial p_j} + \left(\frac{\partial R_g}{\partial\dot{p}_j}\right) = 0, \quad \text{(A10)}$$

where $p_j = \eta, t_p, \phi, \delta$ and $\dot{p}_j = \frac{\partial\eta}{\partial\tau}, \frac{\partial t_p}{\partial\tau}, \frac{\partial\phi}{\partial\tau}, \frac{\partial\delta}{\partial\tau}$, we obtain the coupled ODEs for the CS parameters. These evolution equations are mentioned in Eqs. (9)–(12).

APPENDIX B: DERIVATION OF CS TRAJECTORY UNDER PHASE-MODULATED DRIVING FIELD

We show the simplified coupled equations including only the dominating terms required for tracing the soliton trajectory. The simplified coupled equations are

$$\frac{\partial t_p}{\partial\tau} = \left(-2 + \frac{\pi^3 P_{in}\sin\phi}{4\sqrt{2}\eta^{3/2}}\right)\delta - \left(\frac{M\omega^2 P_{in}\pi^3\sin\phi}{4\sqrt{2}\eta^{3/2}}\right)t_p, \quad \text{(B1)}$$

$$\frac{\partial\delta}{\partial\tau} = -\frac{\pi P_{in}\cos\phi}{\sqrt{2\eta}}\delta + \frac{M\omega^2\pi P_{in}\cos\phi}{\sqrt{2\eta}}t_p. \quad \text{(B2)}$$

We can write it in the form

$$\frac{\partial t_p}{\partial \tau} = A_1\delta - A_2 t_p, \tag{B3}$$

$$\frac{\partial \delta}{\partial \tau} = -B_1\delta + B_2 t_p, \tag{B4}$$

where $A_1 = (-2 + \frac{\pi^3 P_{in}\sin\phi}{4\sqrt{2}\eta^{3/2}})$, $A_2 = (\frac{M\omega^2 P_{in}\pi^3\sin\phi}{4\sqrt{2}\eta^{3/2}})$, $B_1 = \frac{\pi P_{in}\cos\phi}{\sqrt{2\eta}}$, $B_2 = \frac{M\omega^2\pi P_{in}\cos\phi}{\sqrt{2\eta}}$. The set of coupled differential equations can be easily decoupled and we can get a second-order differential equation of t_p of the form

$$\frac{\partial^2 t_p}{\partial \tau^2} + D_1\frac{\partial t_p}{\partial \tau} + D_2 t_p = 0, \tag{B5}$$

where $D_1 = (A_2 + B_1) = \frac{M\omega^2 P_{in}\pi^3\sin\phi}{4\sqrt{2}\eta^{3/2}} + \frac{\pi P_{in}\cos\phi}{\sqrt{2\eta}}$, $D_2 = (B_1A_2 - A_1B_2) = \frac{\sqrt{2}M\omega^2\pi P_{in}\cos\phi}{\sqrt{\eta}}$. Now, the solution of the above equation can simply be written as $t_p(\tau) = Xe^{m_1\tau} + Ye^{m_2\tau}$, where $m_{1,2} = [-D_1 \pm D_1(1-4\Delta)^{1/2}]/2$, with $\Delta = D_2/D_1^2$ and X, Y are constants. Note that if Δ is very small (as $M\omega^2 \ll 1$) then $m_1 \approx -D_2/D_1$ and $m_2 \approx -D_1(1-\Delta)$. Now the boundary conditions $t_p(0) = t_0$ and $v_d(0) = 0$ lead to $X = t_0(1+\Delta)$ and $Y = -\Delta t_0$. Now neglecting Δ and A_2 we may have the following approximate expression of the temporal position:

$$t_p \approx t_0\exp(-2M\omega^2\tau). \tag{B6}$$

APPENDIX C: CALCULATIONS FOR THE REDUCED LAGRANGIAN AND RDF IN CASE MENTIONED IN SEC. IV

To obtain the evolution equations of two CSs we follow the same procedure mentioned in Appendix A.

Step 1. For the two-soliton interaction problem we choose our ansatz as follows.

For soliton 1:

$$\psi_1(t,\tau) = \sqrt{2\eta_1(\tau)}\,\mathrm{sech}\{\sqrt{\eta_1(\tau)}[t - t_1(\tau)]\} \times \exp\left(i\{\phi_1(\tau) - \delta_1(\tau)[t - t_1(\tau)]\}\right), \tag{C1}$$

The interaction between two solitons is mediated with the tail oscillations, therefore we approximate ψ_2 in the following form:

$$\psi_2(t,\tau) \approx 2\sqrt{2\eta_2}\exp\{-\sqrt{\eta_2}[t - t_2(\tau)]\} \times \exp(i\{\phi_2(\tau) - \delta_2(\tau)[t - t_2(\tau)]\}), \tag{C2}$$

The explicit form of the EL equation is

$$\frac{d}{d\tau}\left(\frac{\partial L}{\partial \psi^*_{1\tau}}\right) + \frac{d}{dt}\left(\frac{\partial L}{\partial \psi^*_{1t}}\right) - \frac{\partial L}{\partial \psi^*_1} + \left(\frac{\partial R}{\partial \psi^*_{1\tau}}\right) = 0. \tag{C3}$$

Considering $\psi = \psi_1 + \psi_2$, we can write the LLE for ψ_1 as

$$i\frac{\partial \psi_1}{\partial \tau} + \frac{\partial^2\psi_1}{\partial t^2} + |\psi_1|^2\psi_1 + 2|\psi_1|^2\psi_2 + \psi_1^2\psi_2^* - \sigma\psi_1 + i\psi_1 - iP_{in} = 0. \tag{C4}$$

We choose the form of Lagrangian (L) and RDF (R) functions in such a way that the EL equation for ψ_1 will give back the LLE for ψ_1 as mentioned in C4:

$$L = \frac{i}{2}(\psi_1\psi^*_{1\tau} - \psi_{1\tau}\psi^*_1) + |\psi_{1t}|^2 - \frac{1}{2}|\psi_1|^4 + \sigma|\psi_1|^2, \tag{C5}$$

$$R = (2|\psi_1|^2\psi_2 + \psi_1^2\psi_2^*)\psi^*_{1\tau} + (2|\psi_1|^2\psi_2^* + \psi_1^{*2}\psi_2)\psi_{1\tau} + i(\psi_1\psi^*_{1\tau} - \psi_{1\tau}\psi^*_1) - iP_{in}(\psi^*_{1\tau} - \psi_{1\tau}). \tag{C6}$$

Step 2. Now we integrate the Lagrangian and Rayleigh's function over the fast time (t):

$$L_g = \int_{-\infty}^{\infty} L\,dt, \tag{C7}$$

$$R_g = \int_{-\infty}^{\infty} R\,dt. \tag{C8}$$

The forms of Lagrangian (L_g) and RDF (R_g) are as follows:

$$L_g = 4\sqrt{\eta_1}\left(\delta_1\frac{\partial t_1}{\partial \tau} + \frac{\partial \phi_1}{\partial \tau_1} - \frac{\eta_1}{3} + \sigma + \delta_1^2\right), \tag{C9}$$

$$\begin{aligned} R_g = {} & 8\sqrt{\eta_1}\left(\delta_1\frac{\partial t_1}{\partial \tau} + \frac{\partial \phi_1}{\partial \tau}\right) + 8\eta_1^{3/2}\eta_2^{1/2}e^{-\sqrt{\eta_2}T}\left[6\cos\theta \times \left(\frac{1}{2\eta_1^{3/2}}\frac{\partial \eta_1}{\partial \tau} - \frac{2}{3}\frac{\partial t_1}{\partial \tau}\right) - 2\sin\theta\left(\frac{2\delta_1}{\sqrt{\eta_1}}\frac{\partial t_1}{\partial \tau} + \frac{2}{\sqrt{\eta_1}}\frac{\partial \phi_1}{\partial \tau} + \frac{1}{\eta_1}\frac{\partial \delta_1}{\partial \tau}\right)\right] \\ & - \frac{\pi^3 P_{in}\delta_1^2\sin\phi_1}{2\sqrt{2}\eta_1^2}\frac{\partial \eta_1}{\partial \tau} + \left(1 - \frac{\pi^2\delta_1^2}{8\eta_1}\right)2\sqrt{2}P_{in}\pi\delta_1 \times \cos\phi_1\frac{\partial t_1}{\partial \delta_1} + \frac{\pi^3\delta_1 P_{in}\sin\phi_1}{\sqrt{2}\eta_1}\left(1 - \frac{5\pi^2\delta_1^2}{24\eta_1}\right) \\ & - \left(\delta_1 P_{in}\frac{\partial t_1}{\partial \tau} + P_{in}\frac{\partial \phi_1}{\partial \tau}\right)\left(2\sqrt{2}\pi\cos\phi_1 - \frac{\pi^3\delta_1^2\cos\phi_1}{2\sqrt{2}\eta_1}\right), \end{aligned} \tag{C10}$$

where $\theta = \phi_1 - \phi_2$ and $T = t_1 - t_2$.

Step 3. Now using the form of L_g and R_g in

$$\frac{d}{d\tau}\left(\frac{\partial L_g}{\partial \dot{p_j}}\right) - \frac{\partial L_g}{\partial p_j} + \left(\frac{\partial R_g}{\partial \dot{p_j}}\right) = 0, \tag{C11}$$

where $p_j = \eta_1, t_1, \phi_1, \delta_1$ and $\dot{p_j} = \frac{\partial \eta_1}{\partial \tau}, \frac{\partial t_1}{\partial \tau}, \frac{\partial \phi_1}{\partial \tau}, \frac{\partial \delta_1}{\partial \tau}$, we obtain the coupled ODEs for CS parameters. These evolution equations are mentioned in Eqs. (21)–(24).

Similarly, to obtain the evolution equation for the second CS, which was mentioned in Eqs. (25)–(28), we have interchanged the form of ψ_1 and ψ_2 in the ansatz function mentioned in (C1) and (C2) and follow the same procedure to obtain the coupled ODEs for the parameters of the second CS.

APPENDIX D: COUPLED DIFFERENTIAL EQUATIONS OF TWO SOLITON PARAMETERS MENTIONED IN SEC. V

Following the procedures mentioned in Appendix A for single CS propagation under a phase-modulated driving field and in Appendix C two-soliton propagation with a constant driving field one can easily obtain the governing equations of two CS parameters under a phase-modulated driving field. Here are the coupled mode equations for the two CSs:

$$\begin{aligned}\frac{\partial \eta_1}{\partial \tau} &= -4\eta_1 + 16\eta_1\sqrt{\eta_1\eta_2}\exp(-\sqrt{\eta_1}T)\sin\theta + \frac{\sqrt{\eta_1}}{2}\times\left(2\sqrt{2}\pi P_{in} - \frac{\pi^3\delta_1^2 P_{in}}{2\sqrt{2}\eta_1}\right)(\cos\phi_1 + M\sin\phi_1) - \frac{M\omega^2\sqrt{\eta_1}}{4}\\ &\times\left[2\sqrt{2}P_{in}\sin\phi_1\left(\frac{\pi^3}{4\eta_1} + \pi t_1^2\right) - \frac{2\delta_1^2 P_{in}}{\eta_1}\sin\phi_1\left(\frac{\pi^3 t_1^2}{4} + \frac{5\pi^5}{16\eta_1}\right) - \frac{\sqrt{2}\delta_1\pi^3 P_{in}t_1\cos\phi_1}{\eta_1} + \frac{5\sqrt{2}\pi^5\delta_1^3 P_{in}}{24\eta_1^2}t_1\cos\phi_1\right],\end{aligned} \tag{D1}$$

$$\begin{aligned}\frac{\partial \phi_1}{\partial \tau} &= -\sigma + \eta_1 + \delta_1^2 + 12\sqrt{\eta_1\eta_2}\cos\theta\exp(-\sqrt{\eta_2}T) + 4\delta_1\sqrt{\eta_2}\sin\theta\exp(-\sqrt{\eta_1}T) + \frac{\pi^3 P_{in}\delta_1^2}{2\sqrt{2}\eta_1^{3/2}}(\sin\phi_1 + M\cos\phi_1)\\ &+ \frac{5\sqrt{2}M\omega^2\pi^3\delta_1 P_{in}t_1\sin\phi_1}{8\eta_1^{3/2}} - \frac{5\pi^5\delta_1^4 P_{in}M\cos\phi_1}{96\sqrt{2}\eta_1^{3/2}} - \frac{55\sqrt{2}\delta_1^2 P_{in}t_1\pi^5 M\omega^2\sin\phi_1}{192\eta_1^{3/2}}\\ &- \frac{M\omega^2 P_{in}\delta_1^4\cos\phi_1}{12\sqrt{2}\eta_1^{3/2}}\left(\frac{61\pi^7}{64\eta_1} + \frac{5\pi^5 t_1^2}{16}\right) - \frac{M\omega^2 P_{in}\delta_1^2\cos\phi_1\pi^3}{8\eta_1^{3/2}}\left(\frac{25\sqrt{2}\pi^2}{8\eta_1} + \frac{3t_1^2}{\sqrt{2}}\right),\end{aligned} \tag{D2}$$

$$\begin{aligned}\frac{\partial \delta_1}{\partial \tau} &= 8\eta_1\sqrt{\eta_2}\cos\theta\exp(-\sqrt{\eta_1}T) - \frac{\delta_1}{4\sqrt{\eta_1}}\left(2\sqrt{2}\pi P_{in} - \frac{\pi^3\delta_1^2 P_{in}}{2\sqrt{2}\eta_1}\right)(\cos\phi_1 + M\sin\phi_1)\\ &+ \frac{M\omega^2}{4\sqrt{\eta_1}}\left[2\sqrt{2}\pi P_{in}t_1\cos\phi_1 + \sqrt{2}\delta_1 P_{in}\pi t_1^2\sin\phi_1\left(1 - \frac{\delta_1^2\pi^2}{4\sqrt{2}\eta_1}\right) + \frac{3\delta_1 P_{in}\pi^3\sin\phi_1}{2\sqrt{2}\eta_1}\right.\\ &\left. - \left(1 + \frac{5\pi^2}{96\eta_1}\right)\frac{\sqrt{2}\pi^3\delta_1^2 P_{in}t_1\cos\phi_1}{\eta_1}\right],\end{aligned} \tag{D3}$$

$$\begin{aligned}\frac{\partial t_1}{\partial \tau} &= -2\delta_1 - 4\sqrt{\eta_2}\sin\theta\exp(-\sqrt{\eta_1}T) + \frac{\delta_1 P_{in}\pi^3}{4\sqrt{2}\eta_1^{3/2}}(\sin\phi_1 - M\cos\phi_1) - \frac{M\omega^2}{4\sqrt{2\eta_1^3}}\left[P_{in}t_1\pi^3\sin\phi_1 - 2\sqrt{2}\delta_1 P_{in}\cos\phi_1\right.\\ &\left.\times\left(\frac{5\pi^5}{16\eta_1} + \frac{\pi^3 t_1^2}{4}\right) - \frac{5\pi^5\delta_1^2 P_{in}t_1\sin\phi_1}{8\sqrt{2}\eta_1} + \frac{P_{in}\delta_1^3\cos\phi_1}{3\sqrt{2}\eta_1}\times\left(\frac{61\pi^7}{64\eta_1} + \frac{5\pi^5 t_1^2}{16}\right)\right].\end{aligned} \tag{D4}$$

Here, η_1 (η_2), t_1 (t_2), ϕ_1 (ϕ_2), and δ_1 (δ_2) are the corresponding amplitude, position, phase, and frequency shift of the soliton 1 (soliton 2), $\theta = \phi_1 - \phi_2$ and $T = t_1 - t_2$.

The evolution equations for the second CS are

$$\begin{aligned}\frac{\partial \eta_2}{\partial \tau} &= -4\eta_2 - 16\eta_2\sqrt{\eta_2\eta_1}\exp(-\sqrt{\eta_2}T)\sin\theta + \frac{\sqrt{\eta_2}}{2}\times\left(2\sqrt{2}\pi P_{in} - \frac{\pi^3\delta_2^2 P_{in}}{2\sqrt{2}\eta_2}\right)(\cos\phi_2 + M\sin\phi_2) - \frac{M\omega^2\sqrt{\eta_2}}{4}\\ &\times\left[2\sqrt{2}P_{in}\sin\phi_2\left(\frac{\pi^3}{4\eta_2} + \pi t_2^2\right) - \frac{2\delta_2^2 P_{in}}{\eta_2}\sin\phi_2\left(\frac{\pi^3 t_2^2}{4} + \frac{5\pi^5}{16\eta_2}\right) - \frac{\sqrt{2}\delta_2\pi^3 P_{in}t_2\cos\phi_2}{\eta_2} + \frac{5\sqrt{2}\pi^5\delta_2^3 P_{in}}{24\eta_2^2}t_2\cos\phi_2\right],\end{aligned} \tag{D5}$$

$$\frac{\partial\phi_2}{\partial\tau} = -\sigma + \eta_2 + \delta_2^2 + 12\sqrt{\eta_2\eta_1}\cos\theta\exp(-\sqrt{\eta_1}T) + 4\delta_2\sqrt{\eta_1}\sin\theta\exp(-\sqrt{\eta_2}T) + \frac{\pi^3 P_{in}\delta_2^2}{2\sqrt{2}\eta_2^{3/2}}(\sin\phi_2 + M\cos\phi_2)$$
$$+ \frac{5\sqrt{2}M\omega^2\pi^3\delta_2 P_{in}t_2\sin\phi_2}{8\eta_2^{3/2}} - \frac{5\pi^5\delta_2^4 P_{in}M\cos\phi_2}{96\sqrt{2}\eta_2^{3/2}} - \frac{55\sqrt{2}\delta_2^2 P_{in}t_2\pi^5 M\omega^2\sin\phi_2}{192\eta_2^{3/2}}$$
$$- \frac{M\omega^2 P_{in}\delta_2^4\cos\phi_2}{12\sqrt{2}\eta_2^{3/2}}\left(\frac{61\pi^7}{64\eta_2} + \frac{5\pi^5 t_2^2}{16}\right) - \frac{M\omega^2 P_{in}\delta_2^2\cos\phi_2\pi^3}{8\eta_2^{3/2}}\left(\frac{25\sqrt{2}\pi^2}{8\eta_2} + \frac{3t_2^2}{\sqrt{2}}\right), \tag{D6}$$

$$\frac{\partial\delta_2}{\partial\tau} = -8\eta_2\sqrt{\eta_1}\cos\theta\exp(-\sqrt{\eta_2}T) - \frac{\delta_2}{4\sqrt{\eta_2}}\left(2\sqrt{2}\pi P_{in} - \frac{\pi^3\delta_2^2 P_{in}}{2\sqrt{2}\eta_2}\right)\left(\cos\phi_2 + M\sin\phi_2\right)$$
$$+ \frac{M\omega^2}{4\sqrt{\eta_2}}\left(2\sqrt{2}\pi P_{in}t_2\cos\phi_2 + \sqrt{2}\delta_2 P_{in}\pi t_2^2\sin\phi_2\left(1 - \frac{\delta_2^2\pi^2}{4\sqrt{2}\eta_2}\right) + \frac{3\delta_2 P_{in}\pi^3\sin\phi_2}{2\sqrt{2}\eta_2} - \left(1 + \frac{5\pi^2}{96\eta_2}\right)\frac{\sqrt{2}\pi^3\delta_2^2 P_{in}t_2\cos\phi_2}{\eta_2}\right), \tag{D7}$$

$$\frac{\partial t_2}{\partial\tau} = -2\delta_2 - 4\sqrt{\eta_1}\sin\theta\exp(-\sqrt{\eta_2}T) + \frac{\delta_2 P_{in}\pi^3}{4\sqrt{2}\eta_2^{3/2}}(\sin\phi_2 - M\cos\phi_2) - \frac{M\omega^2}{4\sqrt{2\eta_2^3}}\Bigg[P_{in}t_2\pi^3\sin\phi_2 - 2\sqrt{2}\delta_2 P_{in}\cos\phi_2$$
$$\times\left(\frac{5\pi^5}{16\eta_2} + \frac{\pi^3 t_2^2}{4}\right) - \frac{5\pi^5\delta_2^2 P_{in}t_2\sin\phi_2}{8\sqrt{2}\eta_2} + \frac{P_{in}\delta_2^3\cos\phi_2}{3\sqrt{2}\eta_2} \times \left(\frac{61\pi^7}{64\eta_2} + \frac{5\pi^5 t_2^2}{16}\right)\Bigg]. \tag{D8}$$

These sets of eight coupled differential equations (D1)–(D8) help to visualize the evolution of two CS parameters under a phase-modulated driving field.

[1] T. Herr, V. Brasch, J. D. Jost, C. Y. Wang, N. M. Kondratiev, M. L. Gorodetsky, and T. J. Kippenberg, Nat. Photon. **8**, 145 (2014).

[2] J. K. Jang, M. Erkintalo, S. Coen, and S. G. Murdoch, Nat. Commun. **6**, 7370 (2015).

[3] P. Grelu, *Nonlinear Optical Cavity Dynamics: From Microresonators to Fiber Lasers*, 1st ed. (Wiley-VCH, Weinheim, 2016).

[4] Y. Kivshar and G. P. Agrawal, *Optical Solitons: From Fibers to Photonic Crystals* (Academic, New York, 2003).

[5] A. Ankiewicz and N. Akhmediev, *Dissipative Solitons: From Optics to Biology and Medicine* (Springer, Berlin/Heidelberg, 2008).

[6] F. Leo, S. Coen, P. Kockaert, S.-P. Gorza, P. Emplit, and M. Haelterman, Nat. Photon. **4**, 471 (2010).

[7] A. Roy, R. Haldar, and S. K. Varshney, J. Lightwave Technol. **36**, 5807 (2018).

[8] J. K. Jang, M. Erkintalo, J. Schröder, B. J. Eggleton, S. G. Murdoch, and S. Coen, Opt. Lett. **41**, 4526 (2016).

[9] A. G. Griffith, R. K. Lau, J. Cardenas, Y. Okawachi, A. Mohanty, R. Fain, Y. H. Daniel Lee, M. Yu, C. T. Phare, C. B. Poitras, A. L. Gaeta, and M. Lipson, Nat. Commun. **6**, 6299 (2015).

[10] S. Miller, K. Luke, Y. Okawachi, J. Cardenas, A. L. Gaeta, and M. Lipson, Opt. Express **22**, 26517 (2014).

[11] H. Taheri, A. A. Eftekhar, K. Wiesenfeld, and A. Adibi, IEEE Photonics J. **7**, 1 (2015).

[12] J. K. Jang, M. Erkintalo, S. G. Murdoch, and S. Coen, Opt. Lett. **40**, 4755 (2015).

[13] W. J. Firth and A. J. Scroggie, Phys. Rev. Lett. **76**, 1623 (1996).

[14] F. Pedaci, S. Barland, E. Caboche, P. Genevet, M. Giudici, J. R. Tredicce, T. Ackemann, A. J. Scroggie, W. J. Firth, G.-L. Oppo, G. Tissoni, and R. Jäger, Appl. Phys. Lett. **92**, 011101 (2008).

[15] F. Pedaci, P. Genevet, S. Barland, M. Giudici, and J. R. Tredicce, Appl. Phys. Lett. **89**, 221111 (2006).

[16] D. Anderson, Phys. Rev. A **27**, 3135 (1983).

[17] S. Roy, S. K. Bhadra, and G. P. Agrawal, Opt. Commun. **281**, 5889 (2008).

[18] G. P. Agrawal, *Nonlinear Fiber Optics*, 5th ed. (Academic, New York, 2012).

[19] S. C. Cerda, S. B. Cavalcanti, and J. M. Hickmann, Eur. Phys. J. D **1**, 313 (1998).

[20] A. Sahoo, S. Roy, and G. P. Agrawal, Phys. Rev. A **96**, 013838 (2017).

[21] N. N. Akhmediev, A. Ankiewicz, and J. M. Soto-Crespo, Phys. Rev. Lett. **79**, 4047 (1997).

[22] S. Wabnitz, Opt. Lett. **18**, 601 (1993).

[23] X. Yi, Q. F. Yang, K. Y. Yang, and K. Vahala, Opt. Lett. **41**, 3419 (2016).

[24] W. B. Cardoso, L. Salasnich, and B. A. Malomed, Sci. Rep. **7**, 850 (2017).

[25] L. A. Lugiato and R. Lefever, Phys. Rev. Lett. **58**, 2209 (1987).

[26] I. Hendry, W. Chen, Y. Wang, B. Garbin, J. Javaloyes, G.-L. Oppo, S. Coen, S. G. Murdoch, and M. Erkintalo, Phys. Rev. A **97**, 053834 (2018).

[27] Y. K. Chembo and N. Yu, Phys. Rev. A **82**, 033801 (2010).

[28] C. Godey, I. V. Balakireva, A. Coillet, and Y. K. Chembo, Phys. Rev. A **89**, 063814 (2014).

[29] J. M. McSloy, W. J. Firth, G. K. Harkness, and G.-L. Oppo, Phys. Rev. E **66**, 046606 (2002).

[30] P. Parra-Rivas, D. Gomila, P. Colet, and L. Gelens, Eur. Phys. J. D **71**, 198 (2017).

[31] Y. Wang, F. Leo, J. Fatome, M. Erkintalo, S. G. Murdoch, and S. Coen, Optica **4**, 855 (2017).

[32] J. K. Jang, M. Erkintalo, K. Luo, G.-L. Oppo, S. Coen, and S. G. Murdoch, New. J. Phys. **18**, 033034 (2016)
[33] S. Roy and S. K. Bhadra, J. Lightwave Technol. **26**, 2301 (2008).
[34] M. Haelterman, S. Trillo, and S. Wabnitz, Opt. Commun. **91**, 401 (1992).
[35] T. Maggipinto, M. Brambilla, G. K. Harkness, and W. J. Firth, Phys. Rev. E **62**, 8726 (2000).
[36] V. I. Karpman and V. V. Solov'ev, Physica D (Amsterdam) **3**, 487 (1981).
[37] B. A. Malomed, Phys. Rev. A **44**, 6954 (1991).
[38] B. A. Malomed, Phys. Rev. E **47**, 2874 (1993).
[39] N. J. Smith, W. J. Firth, K. J. Blow, and K. Smith, Opt. Lett. **19**, 16 (1994).
[40] A. V. Buryak and N. N. Akhmediev, Phys. Rev. E **51**, 3572 (1995).
[41] A. Maruta and Y. Kodama, Opt. Lett. **20**, 1752 (1995).
[42] A. Hause, H. Hartwig, M. Bohm, and F. Mitschke, Phys. Rev. A **78**, 063817 (2008).
[43] V. V. Afanasjev, P. L. Chu, and B. A. Malomed, Phys. Rev. E **57**, 1088 (1998).
[44] G. S. Parmar, S. Jana, and B. A. Malomed, J. Opt. Soc. Am. B **34**, 850 (2017).
[45] L. Gui, P. Wang, Y. Ding, K. Zhao, C. Bao, X. Xiao, and C. Yang, Appl. Sci. **8**, 201 (2018).
[46] A. G. Vladimirov, S. V. Gurevich, and M. Tlidi, Phys. Rev. A **97**, 013816 (2018).
[47] D. Turaev, A. G. Vladimirov, and S. Zelik, Phys. Rev. Lett. **108**, 263906 (2012).
[48] P. Wang, X. Xiao, and C. Yang, Opt. Lett. **42**, 29 (2017).